COMPARISON OF KINETIC AND EQUILIBRIUM REACTION MODELS IN SIMULATING THE BEHAVIOR OF GAS HYDRATES IN POROUS MEDIA

Michael B. Kowalsky and George J. Moridis

Lawrence Berkeley National Laboratory
1 Cyclotron Road
Berkeley, CA, 94709, USA
e-mail: MBKowalsky@lbl.gov

ABSTRACT

In this study we compare the use of kinetic and equilibrium reaction models in the simulation of gas (methane) hydrates in porous media. Our objective is to evaluate through numerical simulation the importance of employing kinetic versus equilibrium reaction models for predicting the response of hydrate-bearing systems to external stimuli, such as changes in pressure and temperature. Specifically, we (1) analyze and compare the responses simulated using both reaction models for production in various geological settings and for the case of depressurization in a core during extraction; and (2) examine the sensitivity to factors such as initial hydrate saturation, hydrate reaction surface area, and numerical discretization. We find that for systems undergoing thermal stimulation and depressurization, the calculated responses for both reaction models are remarkably similar, though some differences are observed at early times. Given these observations, and since the computational demands for the kinetic reaction model far exceed those for the equilibrium reaction model, the use of the equilibrium reaction model often appears to be justified and preferred for simulating the behavior of gas hydrates.

INTRODUCTION

Gas hydrates are solid crystalline compounds in which gas molecules (referred to as guests) are lodged within the lattices of ice crystals (called hosts). Under suitable conditions of low temperature and high pressure, a gas G will react with water to form hydrates according to

$$G\ (g) + N_H H_2O\ (w) = G \cdot N_H H_2O\ (h), \quad (1)$$

where N_H is the hydration number and h, g, and w refer to hydrate, gas and water, respectively. Of particular interest are methane hydrates ($G = CH_4$), which represent the majority of natural gas hydrates.

The amount of hydrocarbons residing in hydrate deposits is estimated to substantially exceed all known conventional oil and gas resources [*Sloan*, 1998; *Milkov*, 2004; *Klauda and Sandler*, 2005]. Such deposits occur in two distinct geologic settings where the necessary low temperatures and high pressures exist for their formation and stability: in the permafrost and in deep ocean sediments.

Because of the sheer size of the resource and the ever-increasing energy demand, hydrocarbon hydrates are attracting increasing attention as a potential alternative energy resource [*Moridis*, 2003; *Moridis et al.*, 2005a]. With hydrates being strong cementing agents, the geomechanical behavior of hydrate-bearing sediments in response to thermal and mechanical stresses (natural or anthropogenic) is of particular importance in marine systems because it may lead to deteriorating structural integrity of the oceanic sediment formations that support structures such as hydrocarbon production platforms [*Schmuck and Paull*, 1993; *Paull et al.*, 1996; *Moridis and Kowalsky*, 2006]. There is also evidence linking the large-scale behavior of gas hydrates to instances of rapid global warming in the geologic past [*Kennett et al.*, 2000; *Behl et al.*, 2003]. The scientific and economic implications of all these issues have necessitated the development and evaluation of models that can accurately predict behavior of gas hydrates in porous media.

As *Makogon* [1974] indicated, the three main methods of hydrate dissociation are (1) depressurization, in which the pressure P is lowered to a level lower than the hydration pressure P_e at the prevailing temperature T; (2) thermal stimulation, in which T is raised above the hydration temperature T_e at the prevailing P; and (3) the use of inhibitors (such as salts and alcohols), which causes a shift in the P_e-T_e equilibrium through competition with the hydrate for guest and host molecules. Dissociation results in the production of gas and water, with a commensurate reduction in the saturation of the solid hydrate phase. For the case of methane hydrates, the dissociation reaction is:

$$CH_4 \cdot N_H H_2O\ (h) = CH_4\ (g) + N_H H_2O\ (w), \quad (2)$$

where the hydration number N_H is approximately 6. Depending on the initial thermodynamic state, the water produced from equation (1) can exist as liquid (the common product of dissociation in geologic systems) or ice.

In predicting hydrate dissociation, two approaches are possible. The first considers the reaction of equation (2) to occur at chemical equilibrium, while the second treats it as a kinetic reaction. The equilibrium relationship between P_e and T_e is

described by Figure 1, which also includes the polynomial expression used for the computation of the P_e-T_e curve [*Moridis*, 2003] in addition to the simplified model of *Kamath* [1984]. In this case, the system is composed of heat and two components (CH_4 and H_2O) that are distributed among four possible phases: the gas phase (composed of CH_4 and H_2O vapor), the aqueous phase (composed of H_2O and dissolved CH_4), the solid ice phase (involving exclusively H_2O), and the solid hydrate phase. Thus, the system always exists at equilibrium, with the occurrence of the various phases and phase transitions determined by the availability and relative distribution of heat and of the two components.

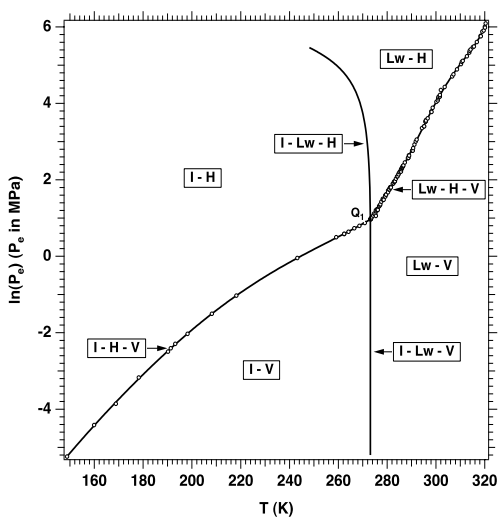

Figure 1. The phase diagram of the water-CH_4-hydrate system [Moridis, *2003*]. *The existence of aqueous (Lw), ice (I), gas (V), and hydrate (H) phases, and combination thereof, are indicated.*

In the kinetic model, the system is composed of heat and three mass components: CH_4 and H_2O, and $CH_4 \cdot N_H\ H_2O$, i.e., the hydrate is not treated as a thermodynamic state of CH_4 and H_2O but as a distinct compound. In this case the solid hydrate phase is considered to be composed exclusively of the $CH_4 \cdot N_H\ H_2O$ component. Phase changes and transitions are determined by a kinetic rate of dissociation or formation, which acts as a source/sink term and is given by the equation of *Kim et al.* [1987]:

$$\frac{dm_H}{dt} = K_0 \exp\left(\frac{-E}{RT}\right) F_A A\left[f_e - f\right], \qquad (3)$$

where f and f_e are the values of fugacity [Pa] for the pressure at temperature T [C] in the gas phase and at equilibrium, respectively; E is the hydration activation energy [J mol^{-1}]; K_0 is the hydration reaction constant [kg m^{-2} Pa^{-1} s^{-1}]; A is the surface area [m^2] for the reaction; F_A is the area adjustment factor [dimensionless], which accounts for deviations from the assumption of grain sphericity used in calculating A [*Moridis et al.*, 2005a]; and R is the universal gas constant [J mol^{-1} C^{-1}]. Values of K_0 and the E have been determined from laboratory data in pure hydrate systems [*Kim et al.*, 1987; *Clark and Bishnoi*, 2001] and in hydrate-bearing media [*Moridis et al.*, 2005c].

It is difficult to know *a priori* which reaction model, equilibrium or kinetic, is most appropriate for the description of problems of hydrate dissociation in porous media. While the kinetic model may provide increased accuracy in some cases, the use of the equilibrium model may often be justified, due to its computational efficiency (as it involves one less equation than the kinetic one) and because predictions made using both models are in many cases remarkably similar [*Moridis et al.*, 2005a]. Prior to this study, we worked with the assumption that, in general, thermal stimulation is accurately described by an equilibrium model, while a kinetic model may be more appropriate for depressurization-induced dissociation.

The objective of this study is to investigate by means of numerical simulation the conditions under which the use of each of the two models (equilibrium or kinetic) is appropriate, and to evaluate differences in predictions from the two models. Specifically, we aim (1) to investigate whether the rate of CH_4-hydrate dissociation in a variety of realistic situations is limited by kinetics; (2) to compare model predictions obtained by using the kinetic and equilibrium models of dissociation for a wide range of production scenarios and geological settings; and (3) to investigate the relative sensitivity of the two dissociation models to a number of parameters, including domain discretization, initial hydrate saturation and the area adjustment factor F_A (Equation 3).

We investigate three test problems. The first involves production from a Class 3 hydrate accumulation [*Moridis and Collett*, 2004], which is characterized by a hydrate-bearing layer (HBL) underlain and overlain by impermeable layers. Dissociation in Problem 1 is induced by thermal stimulation, in which the temperature of the HBL is increased above the hydration temperature at the prevailing pressure (Figure 1). In Problem 2 we examine production at a constant rate from a Class 1 hydrate accumulation. This type of accumulation is characterized by a HBL overlain by an impermeable layer and underlain by a two-phase zone of water and mobile gas, and was identified as a particularly promising target for gas production [*Moridis and Collett*, 2004; *Moridis et al.*, 2005b]. In Problem 3, we simulate the response of a hydrate-bearing core as it is extracted from in-situ conditions and transported to the surface.

NUMERICAL SIMULATOR

The numerical studies in this paper were conducted using TOUGH-Fx/HYDRATE [*Moridis et al.*, 2005a], which models the nonisothermal hydration reaction, phase behavior and flow of fluids and heat under conditions typical of natural CH_4-hydrate deposits in complex formations. It includes both equilibrium and kinetic models of hydrate formation and dissociation and can handle any combination of the possible hydrate dissociation mechanisms (i.e., depressurization, thermal stimulation, and inhibitor-induced effects). TOUGH-Fx/HYDRATE accounts for heat and up to four mass components (i.e., water, CH_4, hydrate, and water-soluble inhibitors such as salts or alcohols) that are partitioned among four possible phases (gas, liquid, ice or hydrate phases, which may exist individually on in any of 12 possible combinations).

PROBLEM 1: THERMAL STIMULATION IN CLASS 3 HYDRATE ACCUMULATION

The HBL of the Class 3 hydrate accumulation in Problem 1 has a thickness of 10 m and involves a cylindrical domain with a maximum radius r_{max} = 1000 m. The domain was divided into 600 grid blocks in the radial direction, beginning at the well radius r_w = 7.5 cm, and employing a spacing that is Δr = 0.05 m near the well and increases logarithmically with r away from the well. The initial hydrate and aqueous phase saturations (S_h and S_a, respectively) are spatially uniform, with $S_h = S_a = 0.5$, making the gas phase saturation $S_g = 0$.

The most relevant model properties are listed in Table 1. Thermal dissociation is recommended in cases of high initial S_h, which corresepond to drastically reduced permeability (rendering depressurization methods impractical). Thermal stimulation is effected by maintaining the well at a constant pressure (equal to the initial HBL pressure) and an elevated temperature of T_W = 45 ^oC (see Table 1). Heat flows from the well into the HBL mainly by conduction, and its rate declines over time as the temperature in the vicinity of the well increases.

Pressure, Temperature and Phase Saturations

Figure 2 shows the radial distributions of pressure, temperature, and phase saturations after 30 days of heating, as obtained from simulations performed using the kinetic and equilibrium reaction models.

By this time, the temperature front (Figure 2a) has propagated into the HBL and induced dissociation over a radius r = 1.3 m, resulting in the evolution of gas (originating exclusively from the hydrate, Figure 2b) and an increase in pressure (Figure 2a). In the region behind the dissociation front (at r < 1.3 m), the hydrate has completely dissociated (S_h = 0), while the saturations S_h and S_g (i.e., of the products of dissociation) have both increased (Figure 2b) over their initial level. We observe a sharp increase in S_h over a short distance immediately ahead of the dissociation front (at r > 1.3 m), mirrored by a corresponding sharp decline in S_a. This is caused by secondary hydrate formation in front of the advancing front, caused by (a) outward flow of a fraction of the released toward the HBL outer boundaries and (b) the increased pressure (Figure 2a) at the dissociation front (caused by the gas release). Past these saturation spikes, the phase saturations remain nearly equal to the initial conditions. Note that the pressure rise at the dissociation front represents a slight increase over the initial pressure; it indicates fluid flow in both directions. Note that the temperature distribution (Figure 2a) is marked by a slight discontinuity in the vicinity of the front.

The most important observation from the review of Figure 2 is that, although slight deviations in the phase saturations and pressure are observed near the dissociation front (where the saturation spikes are observed), the profiles obtained from the kinetic and equilibrium reaction models are nearly identical.

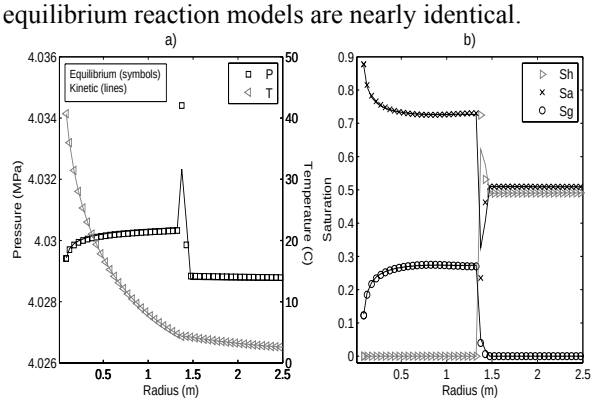

Figure 2. Simulated distributions at 30 days in Class 3 hydrate accumulation undergoing thermal stimulation: (a) pressure P and temperature T; and (b) hydrate saturation S_h, aqueous saturation S_a, and gas saturation S_g. Ice formation does not occur during this simulation (Si = 0).

Gas Release and Production Patterns

Figure 3 shows the gas release and production patterns for the kinetic and equilibrium dissociation models during the 30-day heating period. Specifically, the following quantities are examined: (i) the volumetric rate Q_R of CH_4 release into the formation (Figures 3a); (ii) the volumetric rate Q_P of CH_4 production at the well (Figures 3b); and (iii) the cumulative volumes V_R and V_P of CH_4 released in the formation and produced at the well, respectively (Figures 3c).

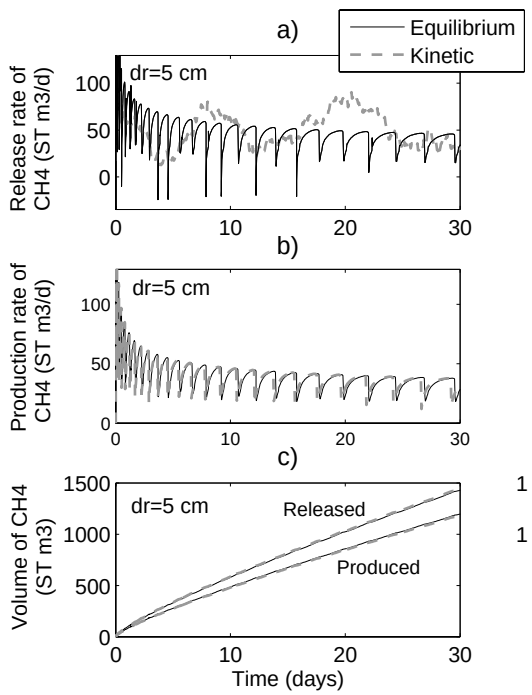

Figure 3. System response to thermal stimulation. The volumetric rate of CH_4 (a) released from the formation, (b) produced at the well, and (c) the corresponding total volumes of CH_4 released from the accumulation and produced at the well.

The rate of CH_4 released to the system during thermal stimulation is shown in Figure 3a. To facilitate comparison between the kinetic and equilibrium release rates, the rates for the kinetic case are averaged in time using a moving window of 5 days. For both cases, Q_R is similar, approximately 50 m^3/day.

The periodic nature of Q_R in the equilibrium case (Figure 3a) is related to the spatial discretization of the domain. As the temperature front propagates into the system, individual grid blocks begin to warm sequentially. Dissociation in a given grid block begins when T increases above the hydration temperature T_e at the prevailing pressure P. Initially Q_R increases with time as the grid block gets warmer. The Q_R increase continues until hydrate dissociation has reduced S_h below a certain critical level, at which point an increasing fraction of the incoming heat is expended to increase the temperature of the porous medium instead of fueling dissociation. Q_R begins to decrease past that point. Additionally, dissociation does not progress significantly into the next grid block because of the steepness of the dissociation front (see Figure 2). Thus, the hydrate dissociation pattern exhibits the sinusoidal/periodic pattern observed in Figures 3a and 3b, in which periodicity coincides with the time for dissociation of a cell in the 1D radial system.

Note that Q_R becomes negative at some times (Figure 3a). This phenomenon results from the fact that the pressure increase caused by dissociation in a grid block causes gas to migrate into the adjacent grid block beyond the dissociation front, where the temperature is still relatively low, causing hydrate formation (due to the increased pressure). This explains why the gas hydrate saturation is increased to nearly 0.8 near the dissociation front in Figure 2b. The rate at which CH_4 is produced at the well (Q_P) is expected to be lower than Q_R since what is released to the formation does not reach production well instantaneously. Figure 3b shows that for both the kinetic and equilibrium cases, the production rates are very similar.

Similarly, we compare the total volumes released from the formation and produced at the well for both cases and find them to be nearly identical (Figures 3c). Similar to the discussion above, V_P comprises what reached the well by a given time, and is therefore less than what is released to the system at a given time.

Sensitivity to Initial Hydrate Saturation, Spatial Discretization and Reaction Area

In addition to the reference value of hydrate saturation S_h (Table 1), we considered two additional values in order to determine its effect on the system response under equilibrium and kinetic conditions. As is evident from Figure 4, the V_R and V_P predictions using the equilibrium and the kinetic models follow the same pattern as those discussed in the reference case (S_h = 0.5). The V_R and V_P predictions when employing the equilibrium model are practically identical to those from the kinetic model for S_h = 0.75, while the two predictions exhibit only very minor differences for an initial S_h = 0.25.

In order to examine the sensitivity of the results to spatial discretization, we performed a simulation with coarser near-well discretization (0.10 m). In this case the Q_R and Q_P rates and the V_R and V_P volumes are similar for both dissociation models (not shown). Compared to the simulation performed using finer discretization, the periodicity of Q_R approximately doubled (mirroring the increase in Δr) because of the longer time needed for the dissociation front to propagate through the length of each grid block. However, the total volumes released to the system and produced at the well were similar to the finer discretization case.

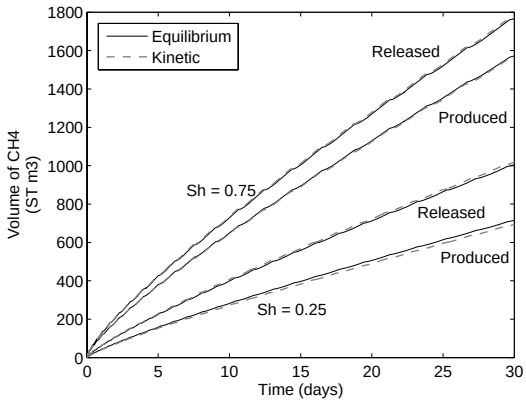

Figure 4. Effect of initial hydrate saturation S_h *on the volume of* CH_4 *released from hydrate formation and produced at the well during thermal stimulation in Class 3 hydrate accumulation. The lower two curves correspond to* $S_h = 0.25$*, while the upper two correspond to* $S_h = 0.75$*.*

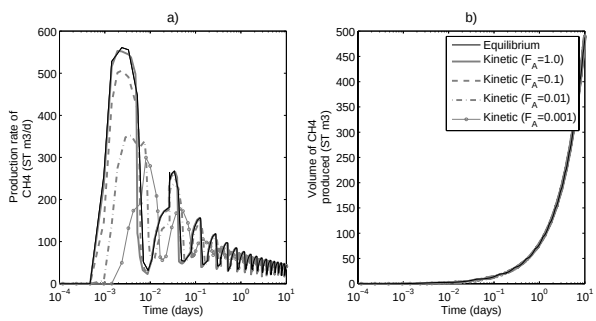

Figure 5. Effect of reaction area on early-time response of Class 3 hydrate accumulation undergoing thermal stimulation. Values of decreasing F_A *are indicated. Initial hydrate saturation* $S_h = 0.5$*.*

Since the area available for heat transfer in the hydration reaction could conceivably cause differences between predictions made using the kinetic and equilibrium reaction models, we conducted a series of simulations with decreasing values of the area adjustment factor F_A (varying from the reference value of 1 to 0.001) to investigate the issue. The results in Figure 5a indicate that a kinetic model with a decreasing F_A results in correspondingly lower production rates Q_P than those predicted in the equilibrium case. However, the Q_P predictions differ substantially only at very early times, and appear to converge for times greater than 1 day. Thus, with the exception of at early times or for very short study periods (e.g., in laboratory studies) Q_P appears to be independent of F_A (Figure 5a) in any practical scenario of thermally-induced dissociation. Note that the early Q_P differences observed for different F_A levels appear inconsequential in the prediction of the overall production volume V_P in Figure 3b, which shows almost complete insensitivity to F_A. This is because the early Q_P differences persist for a very short time and involve very small volumes.

Predictions of thermally-induced gas dissociation and production are practically indistinguishable when using either the kinetic or the equilibrium model (including for varied levels of discretization, initial S_h, and reaction area in the kinetic model), implying that there is no kinetic limitation to gas production from HBL by means of thermal stimulation.

PROBLEM 2: CONSTANT-RATE PRODUCTION IN CLASS 1 HYDRATE ACCUMULATION

This problem involves production in a Class 1 hydrate system in which a 15 meter thick HBL underlies an impermeable layer and overlies a 15 meter thick two-phase zone of gas and water (Figure 6). The upper and lower impermeable layers permit the flow of heat but not fluids.

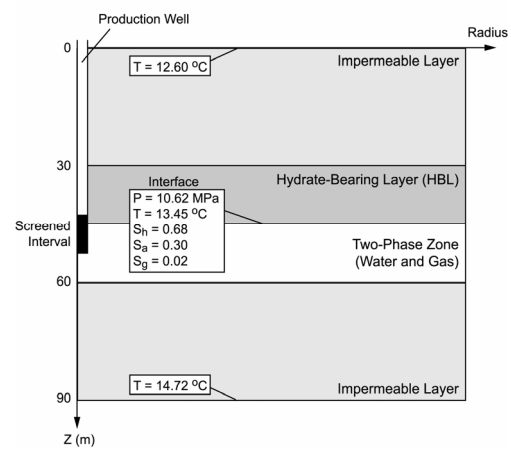

Figure 6. Schematic for Class 1 hydrate accumulation in which constant-rate production is simulated.

The hydrate system is modeled using a 2D cylindrical domain with a maximum radius of 550 m and a vertical span of 90 m. Numerical discretization in the vertical direction equals 25 cm in the HBL and 1 m in the two-phase zone, and ranges between 25 cm and 7 m in the clay layers. Numerical discretization in the radial direction increases from 15 cm to 35 m.

Initially, the hydrate saturation in the HBL is uniform and equals 0.7. The distributions of aqueous and gas saturation in the HBL and in the underlying zone are non-uniform and determined using the equilibration procedure discussed in *Moridis et al.* [2005b]. Fluids are withdrawn at a constant mass rate over a screened portion of the well (see Figure 6).To alleviate the possibility of secondary hydrate formation in the

vicinity of the well during production, heat is added to the well in the entire screened region.

In order to obtain an equilibrated model that maintains the temperature and position (typically known) at the bottom of the HBL, the appropriate boundary conditions and initial conditions must be determined. For this purpose we use a two-step equilibration procedure [*Moridis et al.*, 2005b]. See Table 1 for a description of the model parameters used in this simulation.

Figures 7a-c shows the phase saturation distributions at a simulation time of 60 days. The respective differences between the kinetic and equilibrium models are shown in Figures 7d-f.

System Response during Production

The predicted Q_R curves from the equilibrium and kinetic reaction models over the 2-month simulation period are shown in Figure 8a. During the first day, the Q_R rates for both models are in close agreement; the rate for the kinetic model slightly fluctuates around the smoothly varying rate of the equilibrium model. At later times, Q_R for the kinetic case rises gradually with small-scale fluctuations. In contrast, much larger fluctuations are observed for the equilibrium reaction, beginning at the simulation time of 1 day and continuing for about 45 days, because the equilibrium model is much stiffer and less thermodynamically stable than the kinetic model. Small changes in thermophysical properties and conditions (Pressure, temperature and saturations) can result in fast abrupt changes, introducing slight overshooting of primary variables. This is corrected in the next time step, in which the imbalance caused by the drastic swing is redressed by a condition, state and phase reversal. Figure 8 exhibits the significant fluctuations, which are pronounced during the early stages of production (when the most abrupt changes occur). However, note that these fluctuations revolve about a mean, which very closely follows the kinetic prediction. After 45 days, the kinetic and equilibrium models once again tend toward the same rate.

The released volumes V_R for the kinetic and the equilibrium models (corresponding to the Q_R in Figure 8a) are shown in Figure 8b. The volumes of released gas continuously increase for both cases, though that for the kinetic case initially lags slightly behind (the relative difference is 15% at 60 days, and is likely the maximum deviation to be observed during the simulation); the relative difference between released gas volumes is expected to decrease with simulation times greater than 60 days, considering that release rates have reached a similar level by 60 days (Figure 8a). This is supported by the derivative dV_R/dt values, which are practically identical for the kinetic and equilibrium models by 60 days. The offset in V_R values is caused by the volume accumulations during the abrupt changes at early times (see Figure 8a)

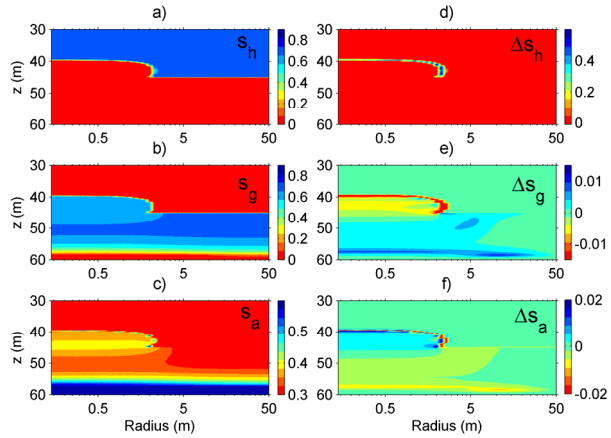

Figure 7. Simulated distributions at 60 days in Class 1 hydrate accumulation undergoing constant-rate production. The hydrate saturation S_h, gas saturation S_g, and aqueous saturation S_a profiles are shown in (a) - (c). The corresponding differences (ΔS_h, ΔS_g and ΔS_a) between profiles simulated using kinetic and equilibrium reaction models are shown in (d) - (f).

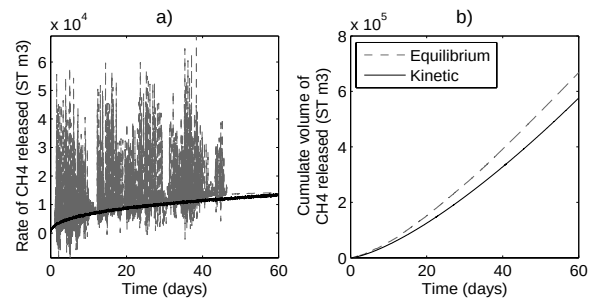

Figure 8. Constant rate production in Class 1 deposit: comparison of CH_4 (a) release rates and (b) total volumes released from the accumulation for equilibrium and kinetic reaction models

As in the case of the first problem, (a) measurable (but still small) deviations between kinetic and equilibrium predictions are observed only at very early times (at which the deviations are at their maximum level), and (b) there appears to be no kinetic limitation to gas production from hydrates by means of depressurization in realistic production scenarios from Class 1 accumulations.

PROBLEM 3: RESPONSE OF HYDRATE-BEARING CORE DURING EXTRACTION

In this problem we study hydrate preservation in an HBL core as it is raised from a depth of 700 m to the surface. Understanding the behavior of hydrate-bearing samples during and after core recovery is of great importance since detection of cores is used in practice to infer the presence and amount of hydrate in the subsurface.

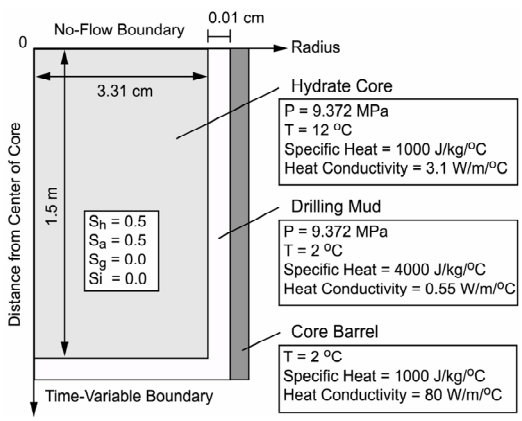

Figure 9. Schematic for hydrate-bearing core simulation. The initial conditions and some relevant parameters for the hydrate core, the drilling mud, and the core barrel are indicated.

The core modeled in this study has a length L = 3.0 m and a radius of 3.13 cm. Neglecting the effects of gravity across the length of the core, we take advantage of symmetry and model only half of it (Figure 9). Using a very fine grid to describe the domain, discretization along the vertical axis ranges between Δz = 0.5 cm and Δz = 1 cm, while discretization along the radial axis was even finer, ranging between Δz = 0.1 cm and Δz = 0.2 cm. A description of the model properties used in this simulation is given in Table 1.

The core is assumed to initially have uniform initial conditions of P = 9.372 MPa and T = 12 °C, and uniform phase saturations of Sh = Sa = 0.5 and Sg = 0. The bottom of the core (and the top, given symmetry) is in contact with drilling mud, which remains at a constant temperature of 2 °C throughout the simulation. (In addition, a thin gap between the core and the mud is modeled at the outer radius of the core, allowing addition contact between the drilling mud and the core.)

To simulate the decreasing pressure to which the core is exposed (and which is the main dissociation-inducing mechanism) as it is raised in the borehole toward the surface, a time-varying boundary condition was applied to the portion of the core in direct contact with the mud. The time-variable boundary involved a linearly decreasing pressure from its initial level of P_0 = 9.372 MPa to the atmospheric pressure (P = 0.101 MPa) over a period of 20 minutes (a reasonable time for the core to reach the surface).

Evolution of Phase Saturations

The evolution of the phase saturations with time, as predicted by the equilibrium model, is shown in Figure 10. No hydrate dissociation is observed in the first 12.5 minutes of core ascent in the wellbore. At time t = 15 min, the effects of dissociation are evident (Figure 10a), and are most pronounced at the parts of the core in direct contact with the variable-pressure boundary, i.e., the core ends (top or bottom, given the symmetry of the problem) and the outer perimeter of the core (where the core holder provides an imperfect seal). Hydrate dissociation then proceeds rapidly, advancing by 0.4 m in 2.5 min (from t = 15.0 min to t = 17.5 min), and another 0.35 m in the next 2.5 min (from t = 17.5 min to t = 20 min).

This problem differs from the previous problems in that the formation of ice occurs. Ice forms because of the rapid temperature drop caused by the strongly endothermic reaction of hydrate dissociation (Figure 10b). The water saturation (Figure 10c) decreases in the regions where both ice formation and gas evolution occur because it is expelled as ice expands. The expelled water accumulates near the perimeter of the core holder and at the ends of the core (depicted as the bottom of the domain in Figure 10), where a higher S_a is observed. Note the heterogeneous distribution of the S_i and S_a once ice begins forming.

The corresponding phase saturation distributions for the kinetic reaction model are shown in Figure 10d-f. Note that the onset of hydrate dissociation is delayed (Figure 10d) relative to the equilibrium case. Moreover, dissociation now occurs over a large zone, creating a smooth transition from the hydrate-free region at the bottom of the core to the region where hydrate remains (as opposed to the sharp boundary observed in Figure 10a). The ice distribution is similarly smoothly varying (Figure 10e), as are the distributions of water saturation (Figures 10f).

Similar to Problem 2, thermodynamic instability and abrupt changes occur in response to the imposition of equilibrium model. Because of the small grid blocks and the sensitivity to pressure and temperature, dissociation leads to ice formation and phase distribution adjustments (often abrupt) that satisfy equilibrium. This cannot be corrected within the same grid block in the next time step (because of the inertia of the solid phases, especially ice), but it is expressed in an adjacent grid block, thus keeping the entire system in balance. Thus, the rapid dissociation and emergence of ice significantly change the phase distribution patterns.

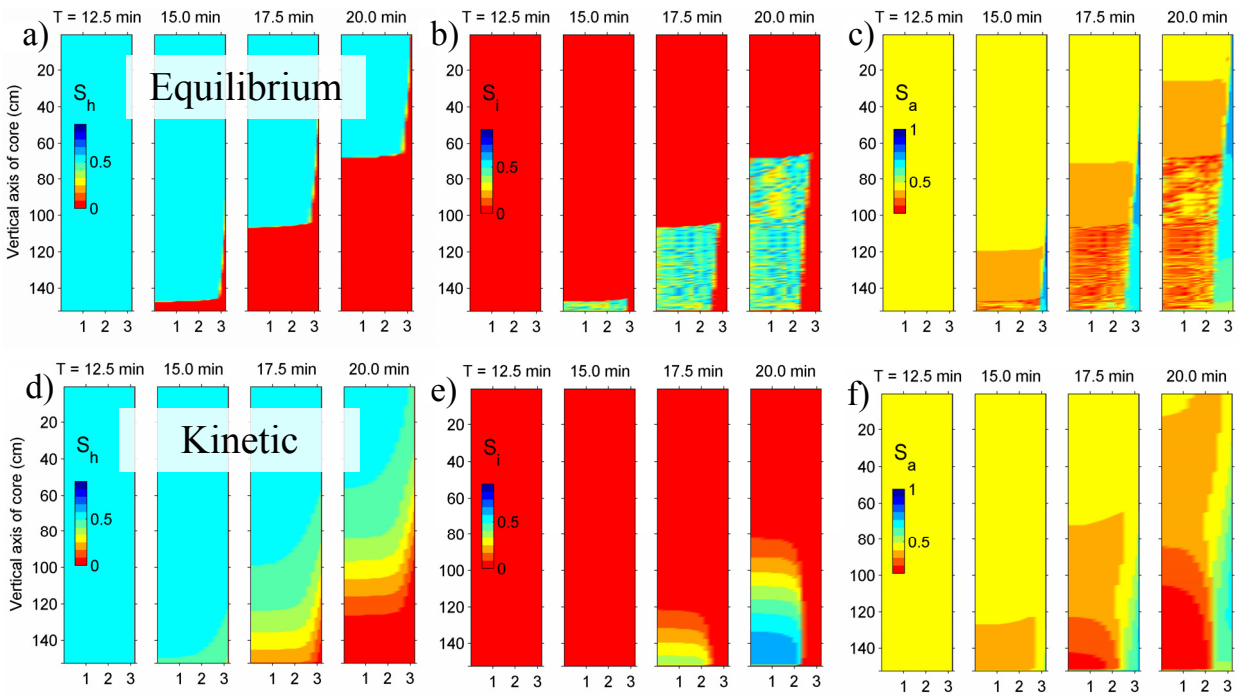

Figure 10. Evolution of the distribution of phases during transport to the surface from a depth of 700 meters simulated using the equilibrium reaction model: a) hydrate saturation S_h*, b) ice saturation* S_i*, c) aqueous phase saturation* S_a*, and d) gas saturation* S_g

System Response during Core Extraction

The rate of methane released from the core during its 20-min ascent to the surface is shown in Figure 11a. The corresponding volume of fraction of CH_4 released from the core during this process is shown in Figure 11b. Note that the use of the equilibrium reaction model for this case would result in a significant overestimation of the amount of hydrate lost during core extraction.

In a short-term process such as the rapid core recovery in this case, kinetic limitations can be important, and ignoring them may lead to serious under-predictions of the recoverable hydrate in cores.

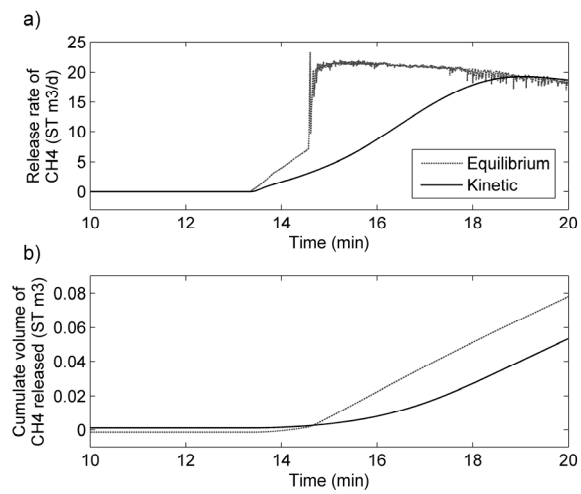

Figure 11. Response of core during transport to the surface from a depth of 700 meters: (a) the rate at which CH_4 *is released from the core and (b) the total volume of* CH_4 *released.*

SUMMARY AND CONCLUSIONS

The objectives of this paper were to evaluate through numerical simulation the importance of employing kinetic versus equilibrium reaction models for predicting the behavior of hydrate-bearing systems in a variety of geological settings.

The first problem involved thermal stimulation in a Class 3 hydrate accumulation. Predictions of thermally-induced gas dissociation and production were practically indistinguishable when using either the kinetic or the equilibrium model (including for varied levels of discretization, initial S_h, and reaction area in the kinetic model), and there appears to be no kinetic limitation to gas production from HBL by means of thermal stimulation.

The second problem considered constant rate production in a Class 1 hydrate accumulation. Measurable but small deviations between kinetic and equilibrium predictions were observed only at very early times. There appears to be no kinetic limitation to gas production from hydrates by means of depressurization in realistic production scenarios from Class 1 accumulations.

The third problem examined the response of a hydrate-bearing core during core-recovery. This case represents one scenario in which the choice of reaction model is of great consequence. In a short-term process, such as the rapid core recovery, kinetic limitations can be important, and ignoring them may lead to serious under-predictions of the recoverable hydrate in cores.

In conclusion, the results of this study indicate that 1) the equilibrium reaction model is a viable alternative to the kinetic model for a wide range of large-scale production simulations; and 2) the kinetic reaction model appears to be important for accurately modeling core-scale simulations.

ACKNOWLEDGEMENT

This work was supported by the Assistant Secretary of Fossil Energy, Office of Natural Gas and Petroleum Technology, through the National Energy Technology Laboratory, under the U.S. Department of Energy, Contract No. DE-AC03-76SF00098. The authors would also like the thank Yongkoo Seol for his careful review and helpful comments.

REFERENCES

Behl, R. J., J. P. Kennett, K. G. Cannariato, and I. L. Hendy (2003), Methane hydrates and climate change; the clathrate gun hypothesis, *AAPG Bulletin*, *87*(10), 1693.

Clark, M. and P.R. Bishnoi (2001), Determination of activation energy and intrinsic rate constant of methane gas hydrate decomposition, Canadian *Journal of Chemical Engineering* 79(1), 143-147.

Corey, A. T. (1954), The interrelation between gas and oil relative permeabilities, *Producers Monthly*, 38-41, November, 1954.

Kamath, V.A. (1984), University of Pittsburgh, Ph.D. Dissertation, Univ, Microfilms Number 8417404.

Kennett, J. P., K. G. Cannariato, I. L. Hendy, and R. J. Behl (2000), Carbon isotope evidence for methane hydrate instability during late quaternary interstadials, *Science*, *288*, 128-133.

Kim, H. C., P. R. Bishnoi, R. A. Heideman, and S. S. H. Rizvi (1987), Kinetics of methane hydrate decomposition, *Chem. Eng. Sci.*, *42*(7), 1645-1653.

Klauda, J. B. and S. I. Sandler (2005), Global Distribution of Methane Hydrate in Ocean Sediment. *Energy and Fuels. 19*, 469-470.

Leverett, M. C. (1941), Capillary Behavior in Porous Solids, *Trans. Soc. Pet. Eng. AIME*, 142, 152-169.

Makogen, Y. F. (1974), *Hydrates of natural gas*.

Milkov, A. V. (2004), Global estimates of hydrate-bound gas in marine sediments: how much is really out there? *Earth Sci. Rev.*, 66 (3-4) pp. 183-197

Moridis, G. J. (2003), Numerical Studies of Gas Production from Methane Hydrates, *SPE Journal*, *32*(8), 359-370.

Moridis, G. J. (2004), Numerical Studies of Gas Production from Class 2 and Class 3 Hydrate Accumulations at the Mallik Site, Mackenzie Delta, Canada, *SPE Reservoir Evaluation and Engineering*, *7*(3), 175-183.

Moridis, G. J. and T. Collett (2004), Gas Production from Class 1 Hydrate Accumulations, in *Recent Advances in the Study of Gas Hydrates*, C. Taylor , J. Qwan, Eds., Kluwer Academic/Plenum, 75-88.

Moridis, G. J., and M. B. Kowalsky (2006), Response of oceanic hydrate-bearing sediments to thermal stress, proceedings in Offshore Technology Conference, Houston, May, 2006.

Moridis, G. J., M. B. Kowalsky, and K. Pruess (2005a), *TOUGH-Fx./Hydrate: A code for the simulation of system behavior in hydrate-bearing geologic media*, LBNL/PUB 3185, Lawrence Berkeley National Laboratory, Berkeley, Calif.

Moridis, G. J., M. B. Kowalsky, and K. Pruess (2005b). Depressurization-induced production from Class-1 Hydrate Deposits, submitted to SPE Journal (97266).

Moridis, G. J., Y. Seol, T. J. Kneafsey (2005c), Studies of reaction kinetics of methane hydrate dissocation in porous media, Proceedings of the Fifth International Conference on Gas Hydrates, Trondheim, Norway, June 13-16.

Paull, C. K., W. J. Buelow, W. Ussler, W. S. Borowski (1996), Increased Continental Margin Slumping Frequency During Sea-Level Low Stands Above Gas Hydrate-Bearing Sediments, *Geology*, *24*, 143.

Pruess, K., C. Oldenburg, and G. Moridis (1999), *TOUGH2 User's Guide, Version 2.0*, Report LBNL-43134, Lawrence Berkeley National Laboratory, Berkeley, Calif..

Schmuck, E. A., and C.K. Paull (1993), Evidence for Gas Accumulation Associated with Diapirism and Gas Hydrates at the Head of the Cape Fear Slide, *Geo-Marine Letters*, 13,145.

Sloan, E. D. (1998), *Clathrate Hydrates of Natural Gases*, Marcel Dekker, Inc., New York, NY.

van Genuchten, M. Th. (1980), A Closed-Form Equation for Predicting the Hydraulic Conductivity of Unsaturated Soils, *Soil Sci. Soc.*, *44*, 892.

Table 1. Parameters for simulations in Class 3 hydrate accumulations.

Parameter	**Problem 1**	**Problem 2**	**Problem 3**
Description of problem	Thermal stimulation in Class 3 hydrate accumulation	Constant-Rate Production in Class 1 hydrate accumulation	Recovery of Hydrate Core from depth of 700 meters
Initial pressure P	4.028×10^6 Pa	*(See text)*	9.372×10^6 Pa
Initial temperature T	1.06 °C	*(See text)*	12 °C
Constant well pressure P_{well}	4.028×10^6 Pa	*N/A*[1]	*N/A*
Constant well temperature T_{well}	45 °C	*N/A*	*N/A*
Production Rate	*N/A*	5.55×10^{-2} kg/s	*N/A*
Heat Injection Rate	*N/A*	12.5 J/s	*N/A*
Initial water saturation S_a	0.5 (0.0509)	*(See text)*	*(See text)*
Initial hydrate saturation S_h	0.5 (0.0491)	*(See text)*	*(See text)*
Initial gas saturation S_g	0.0	*(See text)*	*(See text)*
Porosity	0.30	0.30	0.30
Permeability	2.96×10^{-13} m^2	1.0×10^{-12} m^2	2.96×10^{-13} m^2
Grain density	2,600 kg/m^3	*N/C*[1]	*N/C*
Wet thermal conductivity	3.1 W/m/°C	*N/C*	*N/C*
Dry thermal conductivity	0.5 W/m/°C	*N/C*	*N/C*
Capillary pressure model[2] $P_{cap} = -P_o[(S^*)^{-1/\lambda} - 1]^{-\lambda}$ $S^* = (S_a - S_{a,r})/(S_{a,max} - S_{a,r})$	$S_{a,max} = 1.0$, $\lambda = 0.6$ $P_o = 1{,}887.0$ Pa	*N/A*	$S_{a,max} = 1.0$ $\lambda = 0.45$ $P_o = 2{,}000$ Pa
Capillary pressure model[3] $P_{cap} = -F \cdot G \cdot P_{GE}(S^*)^v$ $F = 1 + A \cdot Bx(a, b, S_H)$ $S^* = (S_a - S_{a,r})/(1 - S_{a,r})$	*N/A*	$v = -0.7$ $A = 9.28$ $a = 2.1$ $b = 2.2$	*N/A*
Relative permeability model[4] $k_{r,a} = [(S_a - S_{a,r})/(1 - S_{a,r})]^n$ $k_{r,g} = [(S_g - S_{g,r})/(1 - S_{a,r})]^n$	$n = 3.0$ $S_{g,r} = 0.02$ $S_{a,r} = 0.12$	$n = 3.0$ $S_{g,r} = 0.02$ $S_{a,r} = 0.25$	$n = 3.0$ $S_{g,r} = 0.01$ $S_{a,r} = 0.06$
Kinetic reaction parameters			
Activation energy E	8.1×10^4 J/mol	*N/C*	*N/C*
Intrinsic rate constant K_0	3.6×10^4 kg m^{-2} Pa^{-1} s^{-1}	*N/C*	*N/C*
Area Factor F_A	1.0	*N/C*	*N/C*

[1] *N/A* indicates that parameter is not applicable; *N/C* indicates no change from corresponding value in Problem 1.
[2] See *van Genucten* (1980) and *Moridis et al.* (2005) for details.
[3] The Brooks-Corey Model (*Corey*, 1954**)** modified to account for effect of hydrate on capillary pressure. *G* is the error function equation that smoothes curve near S^*=0. *Bx* is the incomplete beta function with parameters *a* and *b*. See *Moridis et al.* (2005) for details
[4] The effects of emerging fluid and solid phases on permeability are accounted for using the first Evolving Porous Medium (EPM) model of *Moridis et al.* (2005). The permeability calculated with this model is also used to scale pressure (*Leverett*, 1941).